JOURNAL OF GUIDANCE, CONTROL, AND DYNAMICS
Vol. 20, No. 1, January–February 1997

Pilot-Induced Oscillation Analysis and Prediction with Actuator Rate Limiting

David H. Klyde,* Duane T. McRuer,† and Thomas T. Myers‡
Systems Technology, Inc., Hawthorne, California 90250

A key feature of all of the recent well-recorded severe pilot-induced oscillations (PIOs) is the presence of actuator rate limiting. As part of attempts to develop a comprehensive understanding of PIO phenomena, the results of an effort focused on improved understanding and analysis of actuator rate limiting are presented. For this effort describing functions were used in concert with modern computer simulation techniques to quantify the added phase lag, magnitude reduction, and bandwidth reduction of a rate-limited actuator in terms of the input and actuator design parameters. The results and inverse describing function techniques are then employed to analyze the limit cycle potential of a system that is essentially linear except for the series nonlinearity. The well-documented X-15 landing flare PIO is used to exemplify these analysis techniques. From this example it is shown that these techniques can be used to provide a prediction of the limit cycle or PIO frequency.

Nomenclature

A	= maximum amplitude of actuator command input sine wave
a_1, b_1	= Fourier fundamental coefficients
e	= closed-loop actuator model error
e_L	= rate limit saturation point
K_p	= pilot gain
q	= pitch rate
s	= Laplace operator
T	= linear system time constant
T_{NL}	= nonlinear system indicial response time constant
V_L	= rate limit
δ	= effector output surface position
$\dot{\delta}$	= actuator rate
δ_c	= actuator input position command
δ_h	= horizontal stabilizer angle
θ	= pitch attitude
θ_c	= pitch attitude command
θ_e	= pitch attitude error
$\tau_{p\theta}$	= pitch attitude phase delay
ϕ_i	= phase shift of actuator command input sine wave
ω_a	= linear actuator close-loop bandwidth (or linear actuator gain)
ω'_a	= nonlinear closed-loop actuator bandwidth (or effective nonlinear actuator gain)
$\omega_{\mathrm{BW}_\theta}$	= pitch attitude airplane bandwidth frequency
ω_i	= frequency of actuator command input sine wave
ω_u	= linear system unstable frequency

Introduction

Previous Related Research

THE use of describing functions to analyze the pilot-induced oscillation (PIO) potential of a given pilot-vehicle configuration is by no means a new art. Pioneering work was done over 30 years ago to identify the causes of various PIO phenomena and define appropriate analysis techniques.[1] For cases involving closed-loop actuator rate limiting, approximate describing functions were derived that fully characterized the nonlinearity in approximate terms with three model forms. Their regions of validity were differentiated using a saturation frequency (i.e., presaturation, just saturated, and postsaturation). Recent highly visible events (e.g., YF-22 and JAS 39) have brought about a renewed urgency to more fully understand rate limiting. Recent work in Germany developed a simple sinusoidal input/triangle output describing function that characterizes a rate limiting element (i.e., an infinite bandwidth actuator or a software limit).[2,3] As shown in Ref. 4, this result can also be applied to closed-loop actuator models where the bandwidth frequency of the actuator is much higher than the input frequency. The work presented in this paper steps from these previous efforts to define exact describing functions for the finite bandwidth closed-loop actuator case with rate limiting.

Category II PIOs

The causative factors associated with severe PIOs are many and varied. To identify and treat the diverse key elements it is useful to divide the world of PIOs into appropriate categories. This essentially breaks down a large and complex problem into smaller, more manageable areas. PIOs can range from mild to severe and they can also involve various forms of pilot behavior that require differing analysis procedures. This suggests that PIOs can usefully be classified in categories that are based on existing pilot behavior models and analysis techniques. The result is the proposed categories that are discussed in Refs. 4 and 5. The category associated with actuator rate limiting is summarized next.

In the simplest and best understood type of PIO, both the pilot and effective aircraft dynamics can be characterized with describing functions that are essentially linear (except for simple gain shaping in series with the pilot). These are defined as Category I. Category II PIOs are similar quasilinear pilot-vehicle system oscillations except that series rate or position limits are involved. Rate limiting, either as a series element or as a rate-limited surface actuator, modifies the Category I situation by adding an amplitude-dependent lag and by setting the limit cycle magnitude. These are the most common and easiest to analyze true limit cycle severe PIOs. Category II PIOs are similar to those of Category I except for the dominance of key lag-introducing series nonlinearities that can suddenly come into play when the pilot's input becomes large enough.

Actuator Rate Limiting

A block diagram of a simplified rate-limited actuator model is presented in Fig. 1. The input surface command produces an output surface deflection. The output deflection is fed back to the command to produce an error signal, $e = \delta_c - \delta$. In the forward path the error signal serves as the input to the nonlinear saturation block.

Received Jan. 29, 1996; revision received June 30, 1996; presented as Paper 96-3433 at the AIAA Atmospheric Flight Mechanics Conference, San Diego, CA, July 29–31, 1996; accepted for publication Oct. 17, 1996.

*Senior Research Engineer, 13766 South Hawthorne Boulevard. Senior Member AIAA.
†Chairman of the Board, 13766 South Hawthorne Boulevard. Fellow AIAA.
‡Vice President, 13766 South Hawthorne Boulevard. Senior Member AIAA.

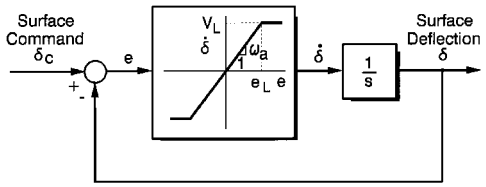

Fig. 1 Closed-loop surface actuator system.

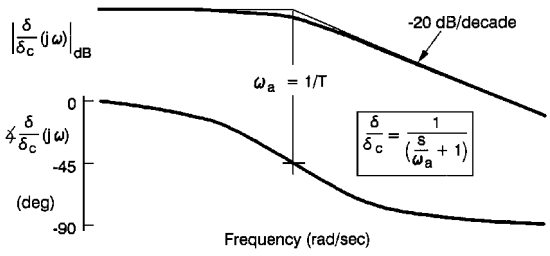

a) Bode plot

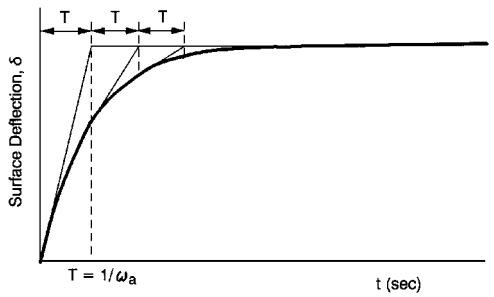

b) Indicial response

Fig. 2 Example linear closed-loop surface actuator response to command.

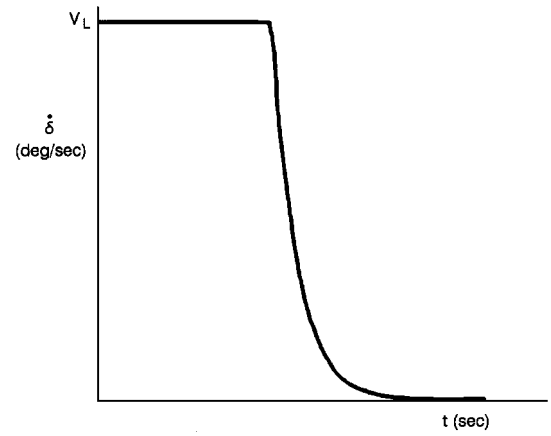

a) Actuator rate

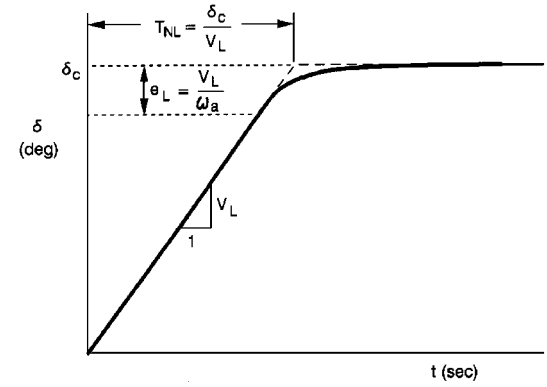

b) Actuator position

Fig. 3 Example nonlinear closed-loop surface actuator response to a δ_c step.

The saturation block is characterized by two design parameters: 1) a gain equivalent to the linear actuator closed-loop bandwidth or more simply referred to as the linear bandwidth and 2) a saturation value equivalent to the actuator rate limit. From Fig. 1 it is clear that the saturation point can be defined in terms of these design parameters by $e_L = V_L/\omega_a$. The output from the saturation block is the surface rate. This signal is then integrated to produce the surface deflection.

The model has three distinct operating ranges. First, when $e < e_L$, the model is linear with a closed-loop response characterized by a simple first-order lag with a time constant, $T = 1/\omega_a$. These first-order features are exemplified in the Bode plot and step time response of Fig. 2. Here everything is characterized by the time constant. Interpreted in the frequency domain, T is the inverse of the linear bandwidth (i.e., the frequency at which the output/input is down 3 dB from the value at zero frequency) as shown in Fig. 2a. In the time domain the indicial response is governed completely by the time constant, e.g., the Fig. 2b exponential response exhibits a series of subtangents that again reflect T. The time constant also corresponds to a system rise time of the indicial response that is determined by the time to reach the maximum (final) surface displacement at the maximum output velocity. One or more of these characteristics is fundamentally changed when the input amplitude exceeds the linear region.

The second operating range is the near saturation range that occurs when the maximum error exceeds e_L by a small amount. This region is characterized by a quasilinear response that is only intermittently rate limited with little associated phase shift. Thus, the nonlinear amplitude effects in this region are imperceptible to the pilot and will not be discussed further.

The third operating range is fully nonlinear and is characterized by an output rate that equals the actuator rate limit, $\dot{\delta} = V_L$, for most of the time. In this highly saturated region the presence of the nonlinearity makes both the frequency and time responses amplitude dependent. For the indicial response, the system rise time (i.e., T_{NL}) will be the magnitude of the step input divided by the velocity limit, as shown in Fig. 3. This defines a step input describing function for the highly saturated case that can be applied to the initial large-amplitude inputs that often precede a fully developed PIO. This rise time is completely independent from that for the linear system. For sinusoidal inputs with amplitudes that are large enough to keep the system velocity at limit values most of the time, the limiter approaches a bang-bang characteristic. As illustrated later, this type of closed-loop system can be characterized by describing functions that can be expressed in simple analytical terms. The bang-bang idealization is a very useful limiting case that is valid when the linear bandwidth is large when contrasted to the effective bandwidth of the nonlinear system. Thus, for this fully nonlinear case, the closed-loop frequency and time response characteristics are totally defined by the rate limit and the input amplitude, independent of the linear system time constant.

The following discussion provides example cases that span the ranges of interest (i.e., linear and highly saturated). For these cases the design parameters ω_a and V_L were held constant at 20 and 40 deg/s, respectively. The input sine wave frequency was held constant at 5 rad/s. The input magnitude of δ_c was varied to obtain responses within the desired range categories. When the design parameters are held constant at these values the system will not saturate until $e = 2$ deg. Also note that for all cases reported here, the input sine wave phase angle was set to zero.

Linear Range

Figure 4a presents the closed-loop actuator model time responses for a linear range case with an input magnitude of 5 deg. The error signal remains below the 2-deg saturation point at all times. The linearity of the response is further exemplified by an actuator rate that is at all times well below the 40-deg/s rate limit. In Fig. 4b the output actuator position is compared to the input command. The noticeable lag in the output response results from the first-order closed-loop time constant as previously identified in Fig. 2. The phase lag due to the effective first-order time constant is $\tan^{-1}(T\omega)$. For the conditions illustrated, this phase lag is well approximated by the argument. Thus, for input frequencies much less than the band-

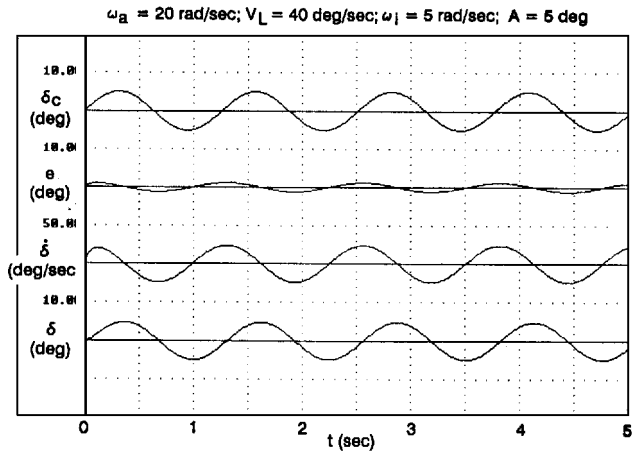

a) Linear system time responses

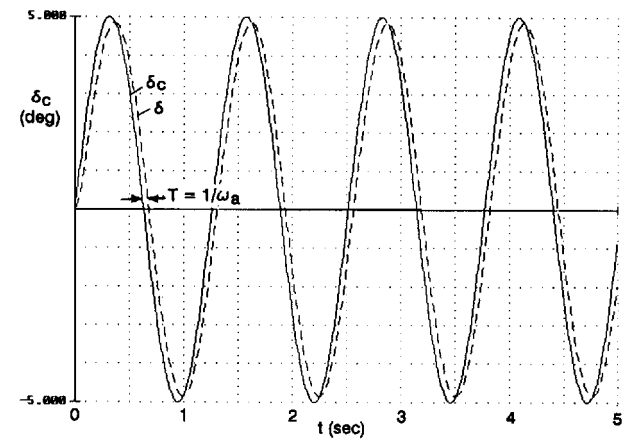

b) Linear system input and output time response comparison

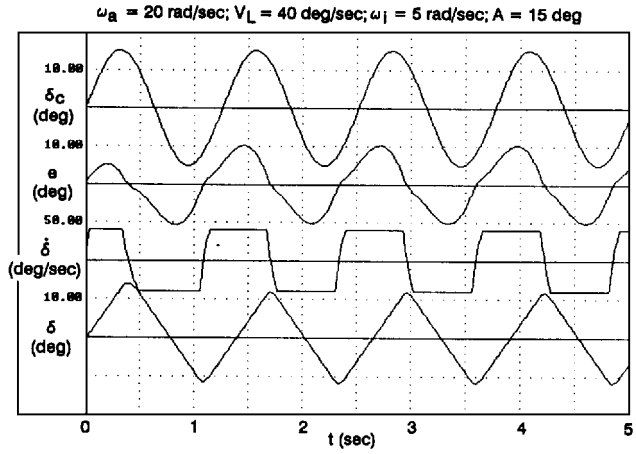

c) Highly saturated system time responses

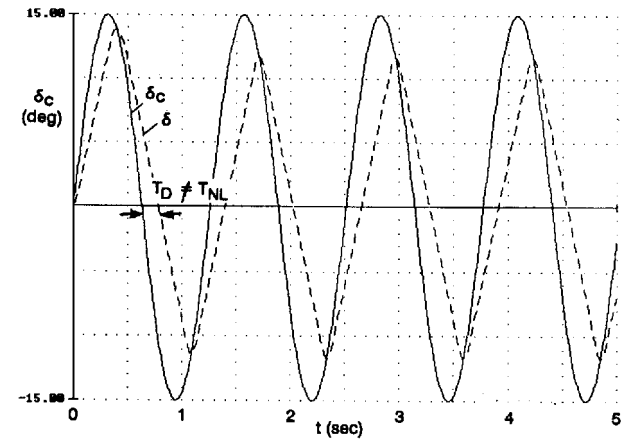

d) Highly saturated system input and output time response comparison

Fig. 4 Closed-loop surface actuator model examples.

width, the output response is shifted from the input by T seconds, as indicated in Fig. 4b.

Highly Saturated

Figure 4c presents the closed-loop actuator model time responses for a saturation case with an input magnitude of 15 deg. The error signal generally exceeds the 2-deg saturation point although it still appears more or less sinusoidal. The nonlinear nature is more evident in the actuator rate response that appears box car-like for this highly saturated case. Thus, the actuator rate operates in a bang-bang (i.e., maximum-to-maximum) fashion. In Fig. 4d the actuator output position is compared to the input command. The figure displays a triangle wave output response that reverses when approximately equal to the input (i.e., when the error signal passes through zero). Unlike the indicial response discussed earlier, the phase lag for this more generalized case is not consistent with T_{NL} (i.e., $\Delta\phi \neq \omega T_{\mathrm{NL}}$). In the analyses that follow, however, it is shown that the T_{NL} parameter still plays a significant role in characterizing the nonlinear system.

Exact Sinusoidal Describing Function

The limitations of the literal approximate describing functions defined in Ref. 4 are their inability to provide an exact phase match to the nonlinear result for the full range of frequencies and time constant ratios. To yield this desired match numerically, an exact sinusoidal describing function is obtained by first computing the Fourier integrals for the input and output fundamentals as defined in Ref. 6 by the following equations:

$$a_1 = \frac{2}{P}\int_{-P/2}^{P/2} f(t)\cos(\omega t)\,\mathrm{d}t \tag{1a}$$

$$b_1 = \frac{2}{P}\int_{-P/2}^{P/2} f(t)\sin(\omega t)\,\mathrm{d}t \tag{1b}$$

In the preceding equations, $f(t)$ is the input or output periodic forcing function that for this case is a sine wave of period P. For sine wave input describing functions the a_1 term for the input is always zero. The a and b terms of Eq. (1) are then used to define the describing function magnitude and phase from Ref. 6 as shown by

$$\left|\frac{\delta(j\omega)}{\delta_c(j\omega)}\right| = \frac{\sqrt{a_{1_{\mathrm{out}}}^2 + b_{1_{\mathrm{out}}}^2}}{b_{1_{\mathrm{in}}}} \tag{2a}$$

$$\angle\frac{\delta(j\omega)}{\delta_c(j\omega)} = -\tan^{-1}\left(\frac{a_{1_{\mathrm{out}}}}{b_{1_{\mathrm{out}}}}\right) \tag{2b}$$

Matlab™/Simulink™ was used to develop a computer simulation of the closed-loop actuator model defined in Fig. 1. To implement the Fig. 1 system, the input was assumed to be sinusoidal, $\delta_c = A\sin(\omega_i t)$. The many time traces given in Appendix A of Ref. 4 support this assumption for PIO cases. To exercise the model, nominal values for the design parameters (ω_a and V_L) and the input parameters (A and ω_i) were first defined. By varying these four parameters systematically, a series of model time responses was obtained. The nonlinear simulation of the Fig. 1 system was then amended to compute the Fourier integrals of Eq. (1) and the magnitude and phase from Eq. (2). In Fig. 5 the exact sinusoidal describing function is compared with the nonlinear simulation for the highly saturated example case of Fig. 4d. As shown in Fig. 5, the describing function provides an exact phase match to the simulation result once the initial transient has passed. This exact phase match occurs because for a sinusoidal input, only the Fourier fundamental is required to completely define the input and output phase (i.e., the higher harmonic terms all share the same phase with the fundamental). The magnitude, however, will in general not be matched unless the remnant harmonic terms are also included. In the Fig. 5 example the describing function peak magnitude falls short of the true nonlinear magnitude by approximately 15%. For full saturation,

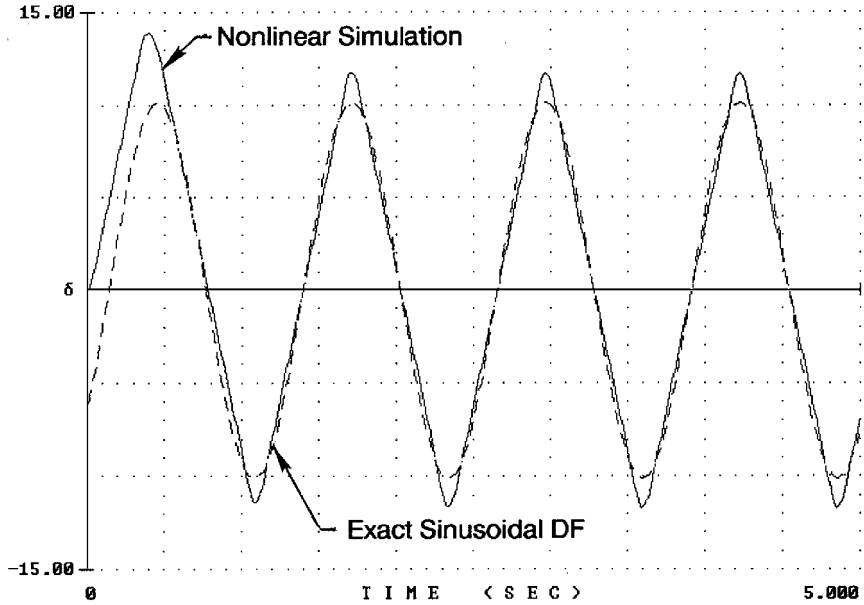

Fig. 5 Exact sinusoidal describing function comparison with the nonlinear simulation: ω_a = 20 rad/s, V_L = 40 deg/s, ω_i = 5 rad/s, and A = 15 deg.

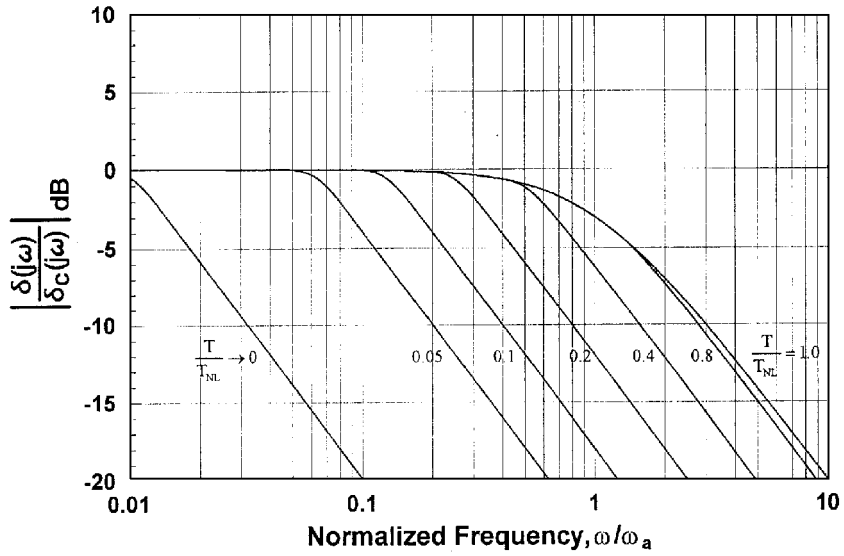

a) Magnitude

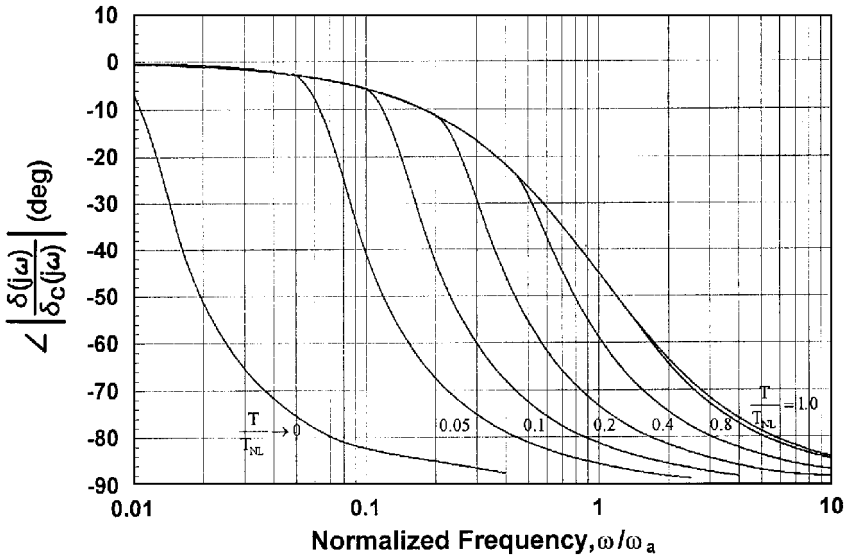

b) Phase

Fig. 6 Exact sinusoidal describing function frequency response.

when the output wave is triangular, the peak of the complete output will be simply $\pi^2/8$ that of the fundamental. Note that the actual peak values of the output wave is irrelevant for stability analyses, whereas the fundamental is essential.

Equation (1) was evaluated numerically to generate the magnitude and phase curve families displayed in Fig. 6. Both sets of curves are plotted as a function of a normalized frequency, ω/ω_a, and the linear to nonlinear time constant ratio, $T/T_{\rm NL}$. In the sinusoidal input case $T/T_{\rm NL}$ is equal to $V_L/(\omega_a A)$. Thus, the two plots display the describing function magnitude and phase of the nonlinear system in terms of the actuator design parameters (V_L and ω_a) and the input parameters (A and $\omega_i = \omega$), all known quantities. There are several observations to note from the plots. First, the $T/T_{\rm NL} = 1$ curve represents the linear case. Second, the more highly saturated cases, represented by the smaller time constant ratio curves, depart from the linear curve at a normalized frequency that is equivalent to their time constant ratio. For example, the $T/T_{\rm NL} = 0.1$ curve departs from the linear curve at a normalized frequency of 0.1. Another more significant result is that known design and input parameters can be used to exactly (i.e., it is exact in relation to the system defined in Fig. 1) identify the added phase lag due to a rate limiting actuator.

Nonlinear Bandwidth

A primary interest in the frequency responses of the describing functions is a search for a useful extension of the linear system bandwidth metrics to the nonlinear case. For the linear first-order case the asymptotic breakpoint of $|\delta/\delta_c|$, at ω_a, is a common linear system bandwidth metric. Thus, an analogous ω_a' becomes an obvious candidate for a nonlinear bandwidth metric. As shown in Fig. 6a, the magnitude frequency response curves for the exact sinusoidal describing function display a first-order-like character in that there is a distinct break frequency defined by the intersection of high- (−20 dB/decade) and low- (0 dB/decade) frequency asymptotes. This break frequency is the defined ω_a'. It is also evident that ω_a' decreases as $T/T_{\rm NL}$ decreases, and $\omega_a' = \omega_a$ for the $T/T_{\rm NL} = 1$ (i.e., linear) case.

To obtain a literal (or symbolic) rather than a graphical representation for the nonlinear bandwidth, describing function approximations must be used. In the following discussion approximations are given for the nonlinear closed-loop actuator bandwidth that are based on the sinusoidal input describing function approximations originally developed in Ref. 1. The rate-limited actuator is approximated in the highly saturated region by a first-order system with a nonlinear bandwidth that is defined as

$$\omega_a' = \frac{1}{\sqrt{[(\pi/4)(A/V_L)]^2 - (1/\omega)^2}} \quad \text{or} \quad \frac{\omega}{\sqrt{[(\pi/4)(A\omega/V_L)]^2 - 1}} \tag{3}$$

This equation can be written in terms of the normalized frequency and the time constant ratio as

$$\frac{\omega_a'}{\omega_a} = \frac{\omega/\omega_a}{\sqrt{[(\pi/4)(T_{\rm NL}/T)(\omega/\omega_a)]^2 - 1}} \approx \frac{4}{\pi}\frac{T}{T_{\rm NL}} = \frac{4}{\pi}\frac{V_L}{\omega_a A} \tag{4}$$

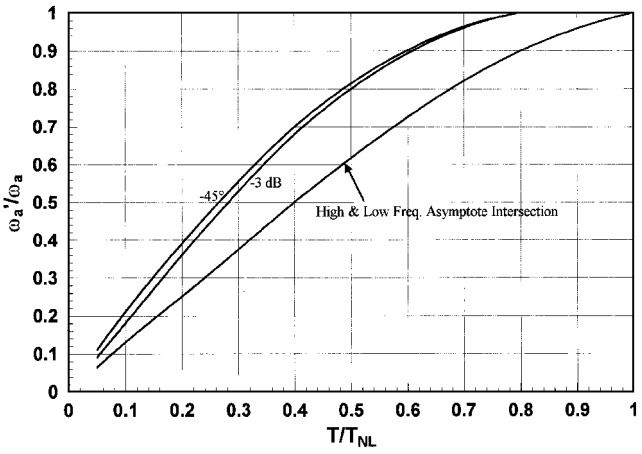

Fig. 7 Nonlinear bandwidth variation.

The simplified form of Eq. (4) applies when the inverse of the time constant ratio is much greater than 1 ($T_{\rm NL}/T \gg 1$). By applying the $\omega_a = 1/T$ identity to the simplified form of Eq. (4), the nonlinear bandwidth is shown to be approximated by a constant with a value near 1 ($4/\pi = 1.273$) times the inverse of the nonlinear time constant. Thus, in the highly saturated region, there is still an analogy to the linear case $\omega_a' \approx (4/\pi)(1/T_{\rm NL})$.

As already described, the nonlinear actuator model displays a first-order-like character. Thus, the nonlinear bandwidth can be defined graphically in terms of classical first-order system measures. In addition to the intersection of the high- and low-frequency asymptotes, these also include the frequency at a phase of −45 deg and at a magnitude of −3 dB. For a linear system these measures, of course, all yield the same bandwidth frequency. As shown in Fig. 7, this is not the case for nonlinear systems. The Fig. 6 exact sinusoidal describing function plots were used to obtain the bandwidth frequencies as a function of $T/T_{\rm NL}$ for the three measures. Figure 7 reveals that the nonlinear bandwidths indicated by the −45 deg and −3-dB curves are nearly identical and larger than those indicated by the asymptote intersection curve. There may be some debate as to which curve appropriately defines the nonlinear bandwidth. Since the asymptote intersection yields a lower frequency, it is the conservative case.

Flying Qualities Cliff

Rate limiting can be particularly insidious because of its highly unexpected and potentially explosive features. At its worst, the phenomenon is a sudden and dramatic incremental shift in the phase lag, equivalent to the sudden insertion of a significant incremental time delay into the loop, initiated by only a slight change in pilot input command. Typically, a well-adapted pilot in an essentially linear pilot-aircraft closed-loop system, operating at high gain to satisfy precision control purposes, is confronted with conditions calling for just a bit more pilot control amplitude or gain. When near the onset or saturation conditions, slight increases in either (or both in combination) are sufficient to enter the nonlinear rate limiting regions, with the concomitant introduction of a sudden phase lag into the closed-loop system. In terms of the underlying physics this is a jump resonance phenomenon.[6] In flying qualities jargon this amounts to a flying qualities cliff.

The Fig. 4 examples can be used to illustrate the jump resonance phenomenon. Assume that the pilot is operating in a high-gain precision control pilot-aircraft system with a corresponding phase margin of about 25 deg. To determine the reduction in phase margin resulting from the rate limiting nonlinearity, the exact describing function is applied. For the highly saturated case that occurs when the input amplitude is increased to 15 deg, there would be a phase shift of −25 deg at this frequency. This will consume all of the available margin and may then result in a limit cycle. This lag will be introduced into the loop as suddenly as the pilot's amplitude is increased. It will typically be unexpected and accordingly quite dramatic giving rise to the cliff metaphor.

Inverse Describing Function Techniques

A key motivation for developing the describing functions defined is to predict closed-loop limit cycles[1] referred to here as Category II PIOs. A synchronous pilot longitudinal closed-loop system with a rate-limited actuator nonlinear element in series with linear elements is given in Fig. 8. As discussed in Ref. 5, when sinusoidal inputs appear in pilot-vehicle systems, a pilot can essentially duplicate the sinusoid with no phase lag up to frequencies of about 3 Hz

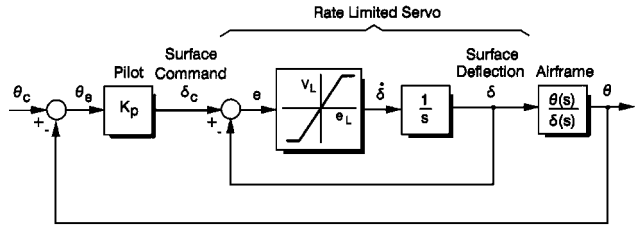

Fig. 8 Synchronous pilot closed-loop system.

(about 20 rad/s). Thus, as shown in the block diagram, the pilot can be represented by a pure gain (K_p). The criterion for a neutrally damped oscillation is simply that the open-loop amplitude ratio is 1.0 (0 dB) and the phase is −180 deg. For an oscillation to persist in the Fig. 8 example, the synchronous pilot system with a series nonlinear element(s) must satisfy the following equation:

$$G(j\omega)N(j\omega, A) = -1 \tag{5a}$$

or

$$G(j\omega) = \frac{-1}{N(j\omega, A)} \tag{5b}$$

In the equation $G(j\omega)$ represents the frequency-dependent linear elements (K_p and θ/δ in Fig. 8) and $N(j\omega, A)$ represents the frequency- and amplitude-dependent onlinear element(s) (the describing function δ/δ_c in Fig. 8).

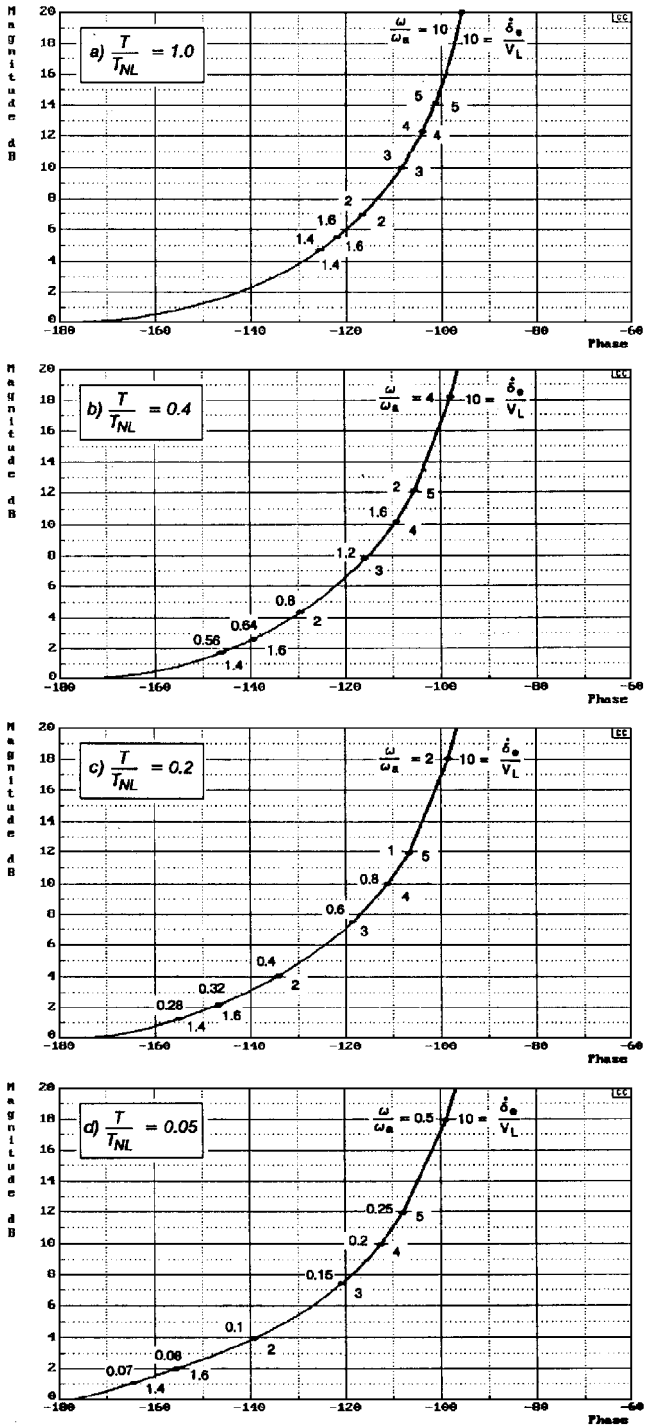

Fig. 9 Exact sinusoidal inverse describing function.

A simple analysis technique[6] is possible when the describing function can be separated from the linear elements, as in the Fig. 8 example. First, the negative inverse describing function [i.e., the right-hand side of Eq. (5b)] is plotted on a standard Nichols or gain-phase chart. The linear portion [i.e., the left-hand side of Eq. (5b)] is then plotted. An intersection of the two curves satisfies Eq. (5b) and provides the frequency and amplitude of the limit cycle.

When ω_a is not necessarily much larger than ω_u, the inverse describing function is a function of amplitude, normalized frequency, and time constant ratio. In Fig. 9 the inverse exact sinusoidal describing function curves are plotted on a Nichols chart for various time constant ratios. Thus, to find the appropriate intersection, the normalized limit cycle frequency, defined by the linear transfer function, must match the normalized frequency of the inverse describing function. The details of applying this method are illustrated by the following example.

X-15 Landing Flare PIO

The X-15 landing/flare PIO occurred on June 8, 1959, with pilot Scott Crossfield. This first flight (designated as Flight 1-1-5) was an unpowered glide flown using the side-located controller with the pitch damper off. Additional details of the flight and subsequent changes to the aircraft are provided in Ref. 7. As shown in the flare time history traces of Fig. 10, severe longitudinal oscillations

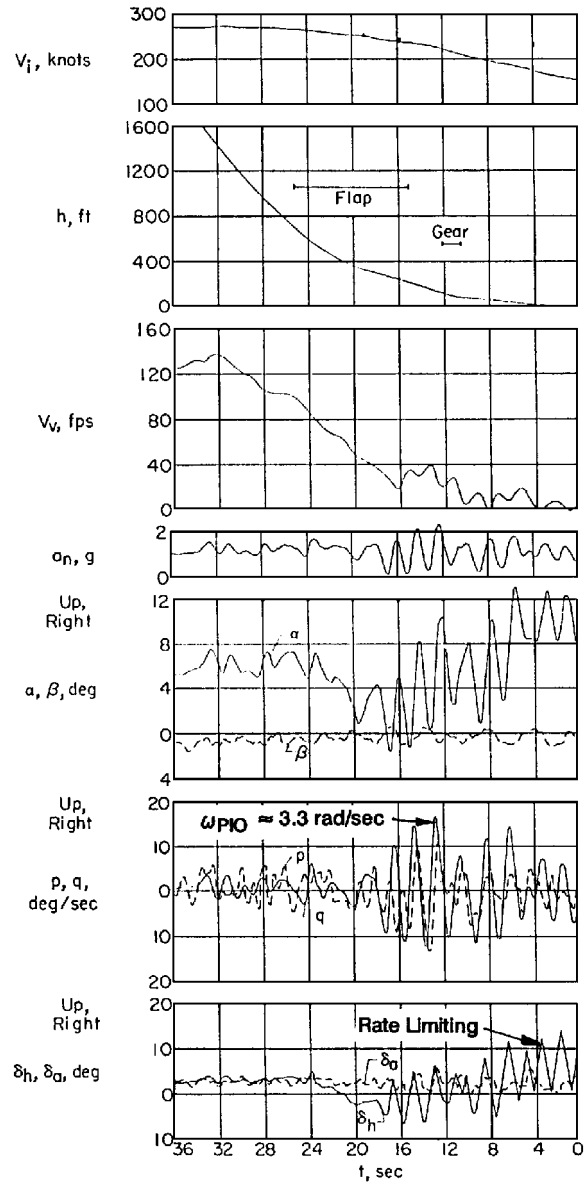

Fig. 10 Time history of the landing flare on X-15 flight 1-1-5 (from Ref. 7).

developed near the end of the flap cycle and rate limiting is clearly evident in the horizontal stabilizer angle trace. The triangle-wave response of the δ_h time trace in the PIO region indicates that the actuator was operating in the highly saturated region. From the pitch rate trace, a PIO frequency of approximately 3.3 rad/s is estimated. For this flight the control surface rate was limited to 15 deg/s.

Since the PIO occurred with the pitch damper off, the X-15 bare airframe data of Refs. 1 and 8 could be used to generate relevant longitudinal transfer functions. Corrections to the Ref. 8 data were made to accommodate the PIO flight condition and aircraft weight. A first-order model for the horizontal stabilizer actuator ($\omega_a = 25$ rad/s) was obtained from Ref. 9. Using these data, the Bode and Nichols frequency response survey of Fig. 11 for the θ/δ_h transfer function was generated. The transfer function gain was arbitrarily set so that the frequency response would pass through 0 dB at -110 deg of phase. Several key Category I PIO indicators (e.g., airplane bandwidth frequency ω_{BW_θ}, phase delay τ_{p_θ}, and average phase rate) are identified on the plots, whereas a more complete accounting of these indicators is given in Appendix B of Ref. 4. As indicated in Ref. 4, not only do all of the applied Category I criteria indicate that the X-15 would not be susceptible to PIO but also the aircraft was found to be level 1 for most of the applied handling qualities measures. Figure 11 also indicates that the instability frequency for the linear system with a synchronous pilot loop closure is 5.31 rad/s. This is considerably larger than the observed PIO frequency of 3.3 rad/s.

Analysis of the X-15 PIO

Inverse describing function techniques are used for single effector with finite bandwidth series nonlinearities to predict limit cycle frequencies and associated added phase lags and magnitude reductions. As discussed earlier, the finite bandwidth case is a function of not only amplitude but also the normalized frequency and time constant ratio (see Fig. 9). The most accurate representation of the nonlinearity is attained with the exact sinusoidal input describing function. This describing function, however, has to be evaluated numerically (this is a simple chore once the describing function is mechanized in a simulation model). More direct but approximate results can be obtained with literal describing function approximations.[4]

The first step in the analysis is to identify the normalized frequency variation on a Nichols chart for the θ/δ_h transfer function. To accommodate possible intersections with the inverse describing function, it is only necessary to identify normalized frequencies for phase angles less than -90 deg, as shown in Fig. 12. These

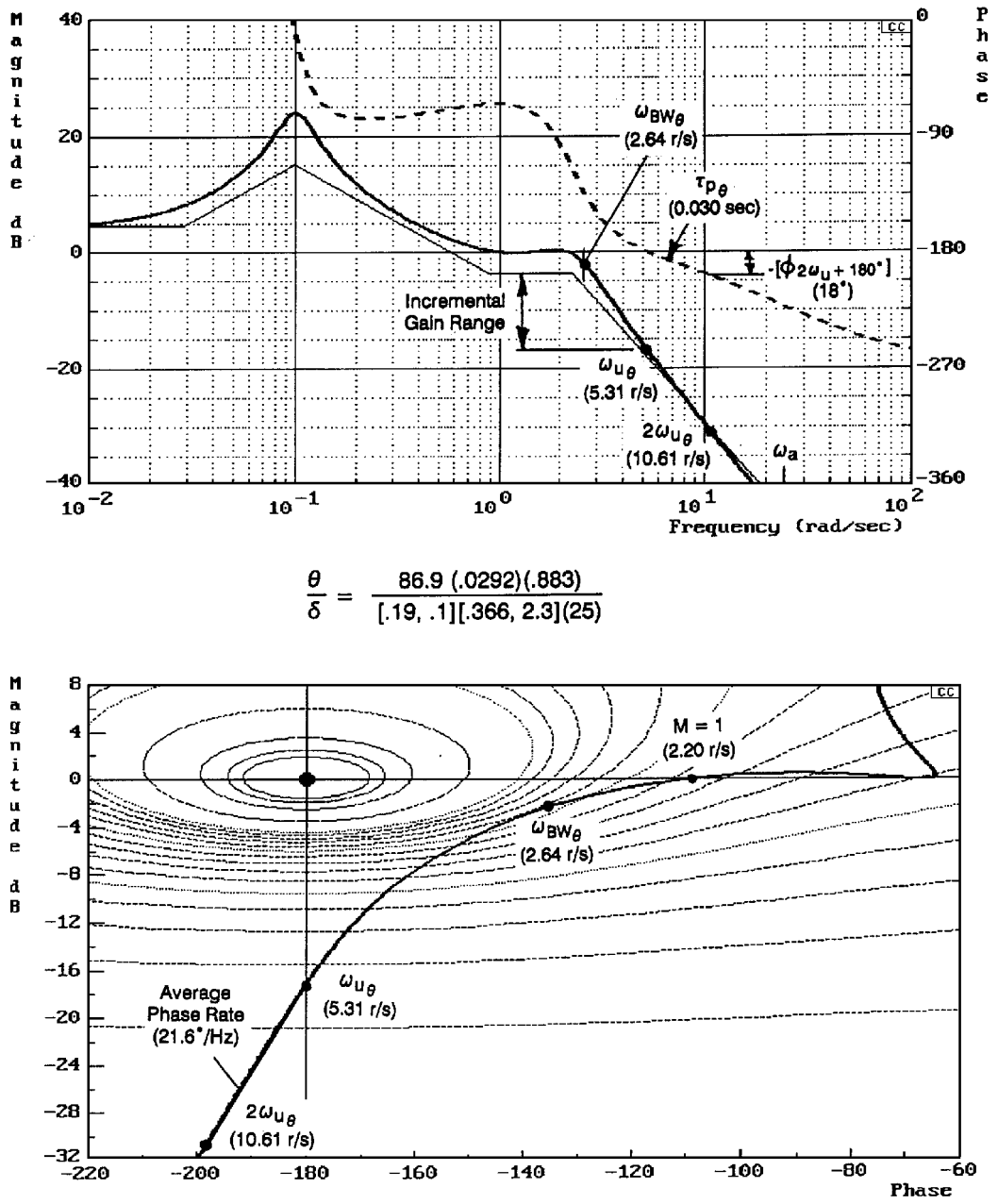

Fig. 11 X-15 pitch attitude (θ/δ) frequency response at the flight 1-1-5 landing flare condition.

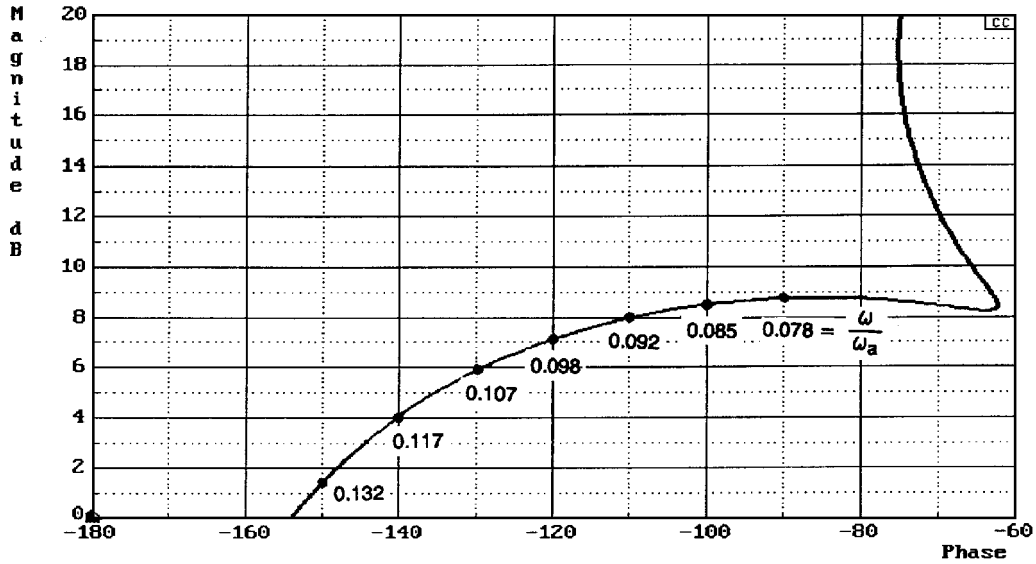

Fig. 12 Normalized frequency variation for the X-15 θ/δ_h transfer function.

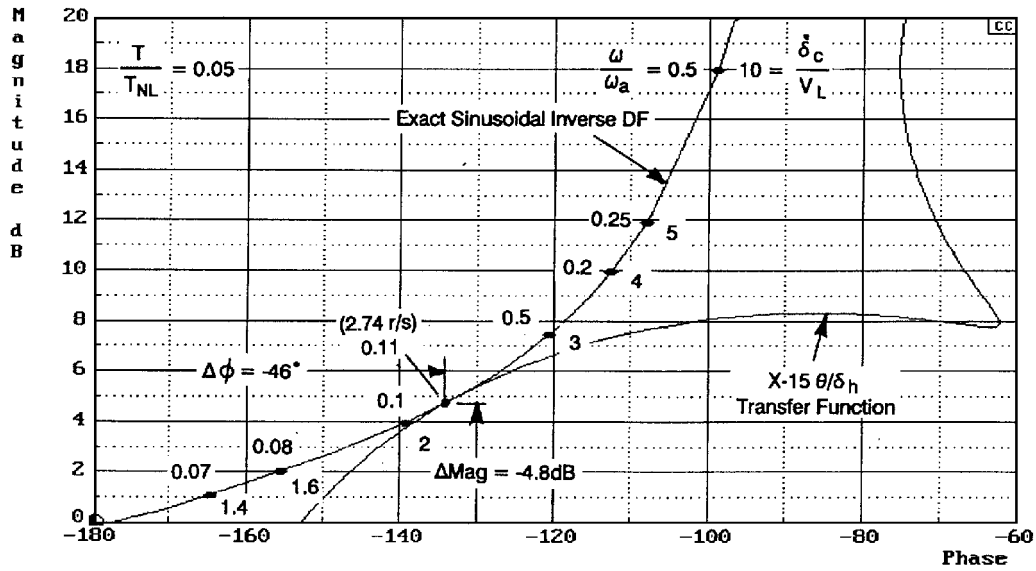

Fig. 13 Limit cycle frequency identification using the sinusoidal inverse describing function with the X-15 example case.

normalized frequencies correspond most closely to the $T/T_{NL} = 0.05$ curve from Fig. 9. To determine the limit cycle frequency, the gain of the X-15 transfer function is adjusted until the curve is just tangent with the inverse describing function curve. The end result is shown in Fig. 13. At the tangent point, a limit cycle frequency of 2.74 rad/s is identified via the linear transfer function, and corresponding values of added phase lag (−46 deg) are read from the plot.

In rate-limited actuators, the added phase lag is accompanied by a significant reduction in actuator bandwidth. The Fig. 7 curves can be used to demonstrate the bandwidth reduction for the X-15 case. The T/T_{NL} value of 0.05 and the −45-deg curve, for example, are used to obtain a ω_a'/ω_a of 0.106. This represents an almost 90% reduction in actuator bandwidth due to rate limiting.

Conclusions

It has been shown that a closed-loop rate limited actuator is characterized by not only an added phase lag but also a significant reduction in actuator bandwidth. Further, the sudden onset of these characteristics can be brought about by only small changes in input amplitude when the pilot is operating in a high-gain closed-loop task. By using the exact describing function analysis methods described in the paper, the characteristics associated with actuator rate limiting that can lead to PIO are quantified in terms of known input and actuator design parameters. For Category II PIO cases where the rate limiting occurs in series with an otherwise linear system, inverse describing function techniques are used to predict the limit cycle or PIO frequency. In the example used here, the PIO frequency was significantly reduced from the linear neutral stability frequency, thus displaying the profound impact of actuator rate limiting. This result takes on added significance in light of the inability of the linear criteria and metrics to identify the PIO susceptibility of this configuration.

Acknowledgments

The material presented here was developed for the U.S. Air Force Flight Dynamics Directorate, Wright Laboratory, as part of the Unified PIO Theory program and is documented in Ref. 4. The Air Force Technical Contact for Systems Technology, Inc., was Charles Suchomel and the Air Force Project Engineer was David B. Leggett.

References

[1]Ashkenas, I. L., Jex, H. R., and McRuer, D. T., "Pilot-Induced Oscillations: Their Causes and Analysis," Northrop Corp., NOR 64-143, Hawthorne, CA, June 1964.

[2]Hanke, D., "Handling Qualities Analysis on Rate Limiting Elements in Flight Control Systems," *Flight Vehicle Integration Panel Workshop on Pilot Induced Oscillations*, AGARD-AR-335, Feb. 1995, pp. 11-1–11-18.

[3]Duda, H., "Frequency Domain Analysis of Rate Limiting Elements in Flight Control Systems," DLR, German Aerospace Research, DLR-FB 94-16, Braunschweig, Germany, 1994.

[4]Klyde, D. H., McRuer, D. T., and Myers, T. T., "Unified Pilot-Induced Oscillation Theory Volume 1: PIO Analysis with Linear and Nonlinear Effective Vehicle Characteristics, Including Rate Limiting," U.S. Air Force Wright Lab., WL-TR-96-3028, Wright–Patterson AFB, OH, Dec. 1995.

[5]McRuer, D. T., "Pilot-Induced Oscillations and Human Dynamic Behavior," NASA CR-4683, July 1995.

[6]Graham, D., and McRuer, D. T., *Analysis of Nonlinear Control Systems*, Wiley, New York, 1961 (also Dover, 1971), Chap. 4.

[7]Matranga, G. J., "Analysis of X-15 Landing Approach and Flare Characteristics Determined from the First 30 Flights," NASA TN D-1057, July 1961.

[8]Heffley, R. K., and Jewell, W. F., "Aircraft Handling Qualities Data," NASA CR-2144, Dec. 1972.

[9]Taylor, L. W., Jr., and Smith, J. W., "An Analysis of the Limit-Cycle and Structural-Resonance Characteristics of the X-15 Stability Augmentation System," NASA TN D-4287, Dec. 1967.